Stem Cell Reports
Article
OPEN ACCESS

# Deterministic *HOX* Patterning in Human Pluripotent Stem Cell-Derived Neuroectoderm

Ethan S. Lippmann,[1,2] Clay E. Williams,[3,4] David A. Ruhl,[5,6] Maria C. Estevez-Silva,[1,2] Edwin R. Chapman,[5,6] Joshua J. Coon,[3,4,7] and Randolph S. Ashton[1,2,*]
[1]Department of Biomedical Engineering
[2]Wisconsin Institute for Discovery
[3]Genome Center of Wisconsin
[4]Department of Biomolecular Chemistry
[5]Department of Neuroscience
[6]Howard Hughes Medical Institute
[7]Department of Chemistry
University of Wisconsin, Madison, WI 53706, USA
*Correspondence: rashton2@wisc.edu
http://dx.doi.org/10.1016/j.stemcr.2015.02.018
This is an open access article under the CC BY-NC-ND license (http://creativecommons.org/licenses/by-nc-nd/4.0/).

## SUMMARY

Colinear *HOX* expression during hindbrain and spinal cord development diversifies and assigns regional neural phenotypes to discrete rhombomeric and vertebral domains. Despite the precision of *HOX* patterning in vivo, in vitro approaches for differentiating human pluripotent stem cells (hPSCs) to posterior neural fates coarsely pattern *HOX* expression thereby generating cultures broadly specified to hindbrain or spinal cord regions. Here, we demonstrate that successive activation of fibroblast growth factor, Wnt/β-catenin, and growth differentiation factor signaling during hPSC differentiation generates stable, homogenous $SOX2^+$/$Brachyury^+$ neuromesoderm that exhibits progressive, full colinear *HOX* activation over 7 days. Switching to retinoic acid treatment at any point during this process halts colinear *HOX* activation and transitions the neuromesoderm into $SOX2^+$/$PAX6^+$ neuroectoderm with predictable, discrete *HOX* gene/protein profiles that can be further differentiated into region-specific cells, e.g., motor neurons. This fully defined approach significantly expands capabilities to derive regional neural phenotypes from diverse hindbrain and spinal cord domains.

## INTRODUCTION

The human genome contains 39 *HOX* genes divided among four clusters and classified into 13 paralogous groups based on sequence homology (Figure 1A). During embryonic stages of body axis elongation, newly formed tissues express *HOX* genes in sequential, contiguous domains consistent with their order in each cluster, i.e., colinearly. This phenomenon is evolutionarily conserved in bilaterian species and spatially assigns body segment-specific differentiation trajectories to axial progenitors of all three germ layers (Lewis, 1978). During formation of the posterior CNS, progenitors proximal to the node progressively transition from a 3′ to 5′ *HOX* expression profile as the primitive streak regresses (Iimura and Pourquié, 2006). This process produces nested and overlapping axial domains of *HOX* expression within the neuroepithelium of hindbrain rhombomeric (*HOX1-5*) and spinal cord cervical (*HOX5-9*), thoracic (*HOX9-10*), and lumbosacral (*HOX10-13*) vertebral segments (Figure 1A) (Philippidou and Dasen, 2013). The spatial variation of *HOX* expression along the rostrocaudal (R/C) axis of the posterior CNS diversifies the fates of neuroepithelial progeny and precisely restricts the development of specific neural subtypes to discrete axial positions (Philippidou and Dasen, 2013).

Retinoic acid (RA), wingless-type MMTV integration site protein family (Wnt), fibroblast growth factor (FGF), and growth differentiation factor (GDF) signaling intricately regulate *HOX* expression during posterior CNS development (Liu et al., 2001; Nordström et al., 2006). Yet, it remains controversial how these factors should be applied to human pluripotent stem cells (hPSCs) to recapitulate full colinear *HOX* activation and enable deterministic patterning of diverse R/C *HOX* profiles, i.e., regional hindbrain or spinal cord phenotypes, during neural differentiation. RA is used ubiquitously to caudalize hPSC-derived neuroectoderm because its secretion by paraxial somitic mesoderm is believed to convert 3′ *HOX* genes in hindbrain and spinal cord neural tissues from an epigenetically repressed to a transcriptionally active state (Gould et al., 1998; Mazzoni et al., 2013; Bel-Vialar et al., 2002). However, RA activates *HOX1-5* chromatin domains in a saltatory (Mazzoni et al., 2013) versus colinear manner, which patterns mouse (mPSC) and human PSC-derived neuroectoderm with a broad caudal hindbrain thru cervical spinal cord identity. This is evidenced by demonstrations that RA-mediated caudalization generates $HOXB4^+$ (Li et al., 2008), $HOXC4^+$/$HOXA5^+$/$HOXC6^-$/$HOXC8^-$ (Mazzoni et al., 2013), $HOXC5^+$/$HOXC6^+$ (Peljto et al., 2010; Wichterle et al., 2002), or $HOXC6^+$/$HOXC8^+$ (Lee et al., 2007; Li et al., 2005) motor neurons (MNs), or

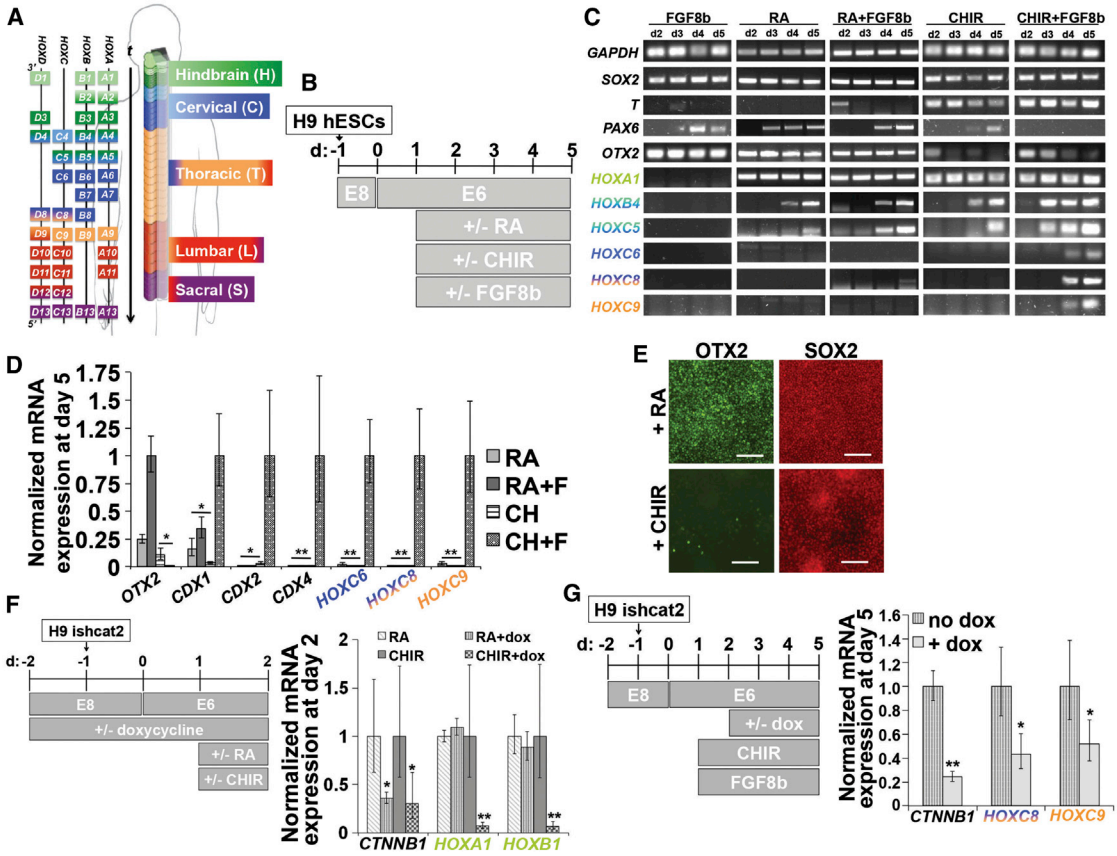


**Figure 1. Wnt/β-Catenin and FGF Signaling Synergistically Coordinate *HOX* Activation during hPSC Differentiation**

(A) *HOX* paralog expression in the hindbrain and spinal cord color-coded to the region where its expression is first detected (modified from a previous report; Philippidou and Dasen, 2013).

(B) Timeline of H9 hESC differentiation corresponding to (C)–(E).

(C) RT-PCR analysis of cultures at days 2–5.

(D) qPCR analysis at day 5. *$p < 0.005$; **$p < 0.001$.

(E) OTX2 and SOX2 expression at day 5 after RA or CHIR treatment. Scale bars, 100 μm. Adjacent images are the same field.

(F) qPCR analysis at day 2 using the H9 ishcat2 line with or without doxycycline treatment. *$p < 0.02$; **$p < 0.005$.

(G) qPCR analysis at day 5 using the H9 ishcat2 line with or without doxycycline treatment. *$p < 0.02$; **$p < 0.0001$.

All qPCR data are presented as mean ± SD calculated from independent biological triplicates. H9 data are normalized to the condition yielding maximum expression and ishcat2 data are normalized to each doxycycline-free condition. Statistical significance was calculated using the Student's unpaired t test.

HOXB4$^+$ astrocytes (Krencik et al., 2011). Alternatively, Wnt and FGF treatments in the absence of RA can caudalize neurally differentiating mPSCs by inducing saltatory activation of *HOX1-9* paralogs to coarsely pattern a heterogeneous mixture of HOXC6$^+$ cervical and HOXD9$^+$ thoracic spinal tissues, which can be further caudalized to also contain HOXD10$^+$ lumbar tissues upon GDF11 supplementation (Mazzoni et al., 2013; Peljto et al., 2010). Also, a recent report demonstrated that manipulation of Wnt and RA concentrations could yield MNs possessing hindbrain or rostral spinal phenotypes but more caudal and further partitioning of regional HOX identity was not achieved (Maury et al., 2014). Overall, an approach for hPSC neural differentiation that recapitulates the precision, extent, and predictability of colinear *HOX* patterning observed in vivo remains elusive. Its development would enable unprecedented access to diverse regional phenotypes that populate posterior CNS tissues and generation of human disease models containing regional neural phenotypes with differential susceptibility to neurodegenerative disorders (Brockington et al., 2013; Kaplan et al., 2014; Sandoe and Eggan, 2013).

Recent progress in understanding how the posterior CNS develops led us to consider other methods for in vitro *HOX* patterning. New evidence suggest that bipotent SOX2$^+$/Brachyury(*T*)$^+$ neuromesodermal progenitors

(NMPs) residing in a stem zone proximal to the primitive streak's regressing node are the cell source for both the posterior neural tube and flanking paraxial mesoderm (Delfino-Machín et al., 2005; Takemoto et al., 2011; Tzouanacou et al., 2009). These NMPs are maintained by synergistic Wnt/β-catenin and FGF signaling from the node and primitive streak that induces SOX2 expression via activation of enhancer N1 (Takemoto et al., 2006, 2011). FGF signaling from the node also helps maintain the NMP state by repressing the expression of the neuroectoderm fate determinant PAX6 (Bertrand et al., 2000; Mathis et al., 2001). As the node regresses, NMPs rostral to the stem zone experience a decline in FGF signaling, which initiates paraxial mesoderm differentiation (i.e., somite formation). Then, the somites secrete RA back to the presumptive neural tube, which induces PAX6 expression to generate definitive neuroectoderm of the posterior CNS (Diez del Corral et al., 2003; Molotkova et al., 2005). The discovery that Wnt/FGF signaling induces NMPs that progressively caudalize *HOX* expression and undergo RA-induced neuroectoderm differentiation to form the hindbrain and spinal cord suggests an alternative approach for patterning *HOX* expression in vitro. Guoti et al. recently had partial success recapitulating the *HOX*-expressing NMP state from hPSCs in vitro, but the NMP phenotype could only be maintained for 3 days preventing acquisition of more caudal HOX genes/proteins before exhibiting a mesodermal shift (Gouti et al., 2014). Also, they were unable to partition *HOX* patterning within hindbrain and spinal cord regions. Therefore, we proceeded to test whether (1) Wnt/β-catenin and FGF signaling could differentiate hPSCs to stable NMPs to permit full, colinear activation of *HOX* genes; (2) RA exposure could differentiate NMPs to neuroectoderm; (3) this approach to deriving human neuroectoderm could enable enhanced control of *HOX* patterning.

Using a chemically defined, monolayer neural differentiation system (Lippmann et al., 2014), we determined that by temporally modulating Wnt/β-catenin and FGF signaling, hPSCs could be differentiated into pure $SOX2^+$/$Brachyury^+$ NMPs that were stable for 7 days. Over this period, the NMPs exhibited colinear activation of hindbrain, cervical, and thoracic *HOX* genes plus lumbosacral *HOX* genes with GDF11 supplementation. At any point during NMP propagation, a transition to RA was necessary and sufficient to induce $PAX6^+$/$SOX2^+$ neuroectodermal differentiation, precisely arrest progressive *HOX* activation, and thereby generate discrete HOX protein profiles indicative of distinct R/C domains. Overall, we demonstrate the ability to deterministically pattern neuroectoderm to diverse R/C domains by simply varying the amount of time NMPs spend under Wnt/β-catenin, FGF, and GDF signaling prior to RA exposure. Furthermore, we demonstrate that neuroectoderm of differing HOX expression profiles produce region-specific hindbrain, cervical, thoracic, and lumbar MN populations. Therefore, this temporal biphasic approach could be used to produce regional neural phenotypes from diverse hindbrain and spinal cord domains.

## RESULTS

### Regulation of *HOX* and *CDX* Expression by RA, Wnt/β-Catenin, and FGF Signaling

We used the chemically defined "E6" method to investigate the effects of Wnt, FGF, RA, and GDF11 during hPSC neural differentiation because it lacks the use of small molecule inhibitors that could influence fate choices and does not form non-neural germ layers that could initiate unknown signaling crosstalk (Lippmann et al., 2014). We first differentiated H9 human embryonic stem cells (hESCs) in E6 medium for 24 hr and then added RA, CHIR99021 (CHIR; a small molecule Wnt/β-catenin agonist), FGF8b, or their relevant combinations and monitored *HOX* expression by RT- and quantitative PCR (qPCR) over 4 days (Figures 1B–1D). The addition of RA or CHIR, but not FGF8b, induced temporal, progressive expression of *HOXA1-HOXC5* (Figure 1C). However, CHIR/FGF8b, but not RA/FGF8b, accelerated the progression of *HOX* activation inducing colinear activation of *HOXC6*, *HOXC8*, and *HOXC9* at levels ranging from 39- to 3,400-fold higher than the other treatments (Figures 1C and 1D). Moreover, the caudalizing effect of CHIR/FGF8b was not impeded by the addition of HX531, an RXR inhibitor, and CHIR but not RA treatment was able to reduce gene and protein expression of the midbrain/forebrain marker *OTX2* (Figures 1C–1E; Figure S1). These results indicate that while RA can induce some degree of posterior identity indicated by *HOX1-5* expression, CHIR/FGF8b induces rapid patterning of differentiating hESCs to an $OTX2^-$ posterior phenotype with caudal *HOX1-9* expression in an RA-independent manner. This is in agreement with other neural differentiation studies (Gouti et al., 2014; Mazzoni et al., 2013)

Additionally, CHIR/FGF8b treatment yielded substantially elevated expression of *CDX* genes, which are the upstream regulators of *HOX* genes (Nordström et al., 2006): compared to RA, CHIR/FGF8b upregulated *CDX1* by >6-fold, *CDX2* by >1,800-fold, and *CDX4* by >330-fold (Figure 1D). To confirm that CHIR-mediated *HOX* induction requires β-catenin signaling, we utilized the H9 ishcat2 line, which harbors a doxycycline-inducible β-catenin small hairpin RNA (shRNA) cassette (Lian et al., 2012). Addition of doxycycline prior to CHIR treatment reduced β-catenin (*CTNNB1*) expression by 3-fold and decreased *HOXA1* and *HOXB1* expression by 14- and 15-fold,

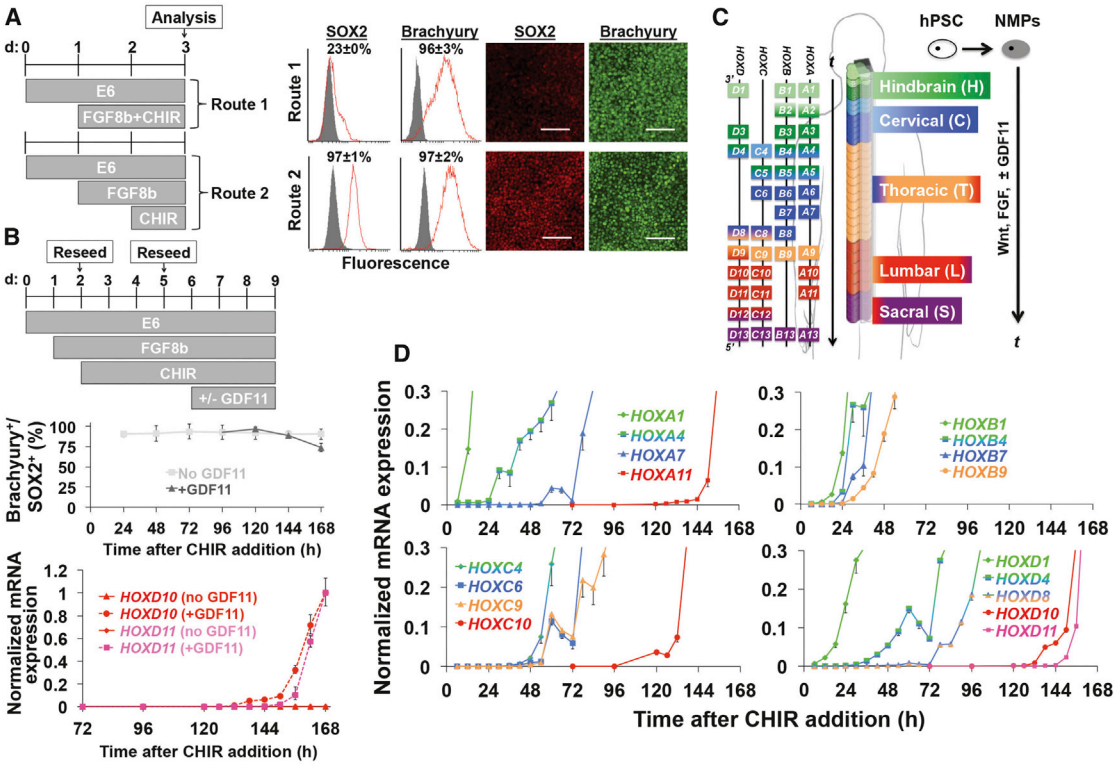


**Figure 2. Colinear *HOX* Expression in hPSC-Derived NMPs**

(A) Analysis of the NMP phenotype by flow cytometry and immunocytochemistry. Gray histogram, immunoglobulin G (IgG) control; red histogram, label of interest. Scale bars, 100 μm.

(B) Optimized NMP propagation scheme. The addition of CHIR is denoted as t = 0 hr in all panels. Purity of NMPs was assessed by flow cytometry in the presence or absence of GDF11 (data are presented as mean ± SD). qPCR analysis of *HOXD10* and *HOXD11* was conducted in the presence or absence of GDF11 (expression normalized to the time point of maximum expression).

(C) Schematic for *HOX* induction in NMPs. "t" indicates time under Wnt, FGF, and GDF signaling.

(D) qPCR analysis of colinear *HOX* expression normalized to the time point of maximum expression. GDF11 was included according to (B). qPCR data in all panels are presented as mean ± SD calculated from technical duplicates. Full profiles for all analyzed genes can be found in Figure S2A. For all flow cytometry data, a minimum of two biological replicates was used to calculate mean ± SD.

respectively (Figure 1F). In contrast, while doxycycline treatment also reduced β-catenin by 3-fold in RA-treated cells, it did not reduce *HOXA1* or *HOXB1* expression, suggesting RA-mediated induction of *HOX* transcription is β-catenin independent (Figure 1F). To verify sustained β-catenin signaling promotes progressive *HOX* activation, we induced *HOX* expression with CHIR/FGF8b for 1 day and continued the treatment for 3 days with and without doxycycline. Doxycycline treatment reduced *CTNNB1* by 4-fold, *HOXC8* by 2-fold, and *HOXC9* by 2-fold, indicating that sustained β-catenin signaling contributes to progressive *HOX* activation (Figure 1G).

## Derivation of Stable NMPs Exhibiting Full Colinear *HOX* Activation

Gouti et al. recently demonstrated that simultaneous induction of Wnt/β-catenin and FGF signaling can differentiate hPSCs to SOX2$^+$/Brachyury($T$)$^+$ NMPs, but NMPs persisted for only 3 days before shifting to a mesodermal fate under their treatment regimen (Gouti et al., 2014). We observed a similar trend with simultaneous CHIR and FGF8b treatment inducing uniform Brachyury but also causing a sharp decrease in SOX2 expression (23% ± 0% SOX2$^+$), indicating a mesodermal fate shift (Figure 2A, Route 1). Conversely, pre-treatment with FGF8b prior to CHIR (pre-FGF8b/CHIR) yielded uniform expression of both Brachyury and SOX2 that could be maintained (75%–100% SOX2$^+$/Brachyury$^+$) for 7 days (Figure 2A, Route 2, and Figure 2B). Thus, FGF signaling upstream of Wnt/β-catenin signaling effectively induces a stable NMP identity during hPSC differentiation.

Next, we investigated whether colinear *HOX* expression was evident within our NMP cultures. Analogous to their in vivo counterparts, these cultures exhibited colinear

activation of *HOX* genes over the 7-day period (Figures 2B–2D; Figure S2). In our system, 3′ *HOX* transcripts remained expressed even after activation of caudal paralogs and fluctuated within an ~5-fold range (Figure S2A), also agreeing with Gouti et al. (2014). Supplementation with GDF11, a transforming growth factor β (TGF-β) family member expressed at later stages of NMP propagation in vivo (Liu, 2006; Liu et al., 2001), was necessary for robust activation of lumbosacral *HOX* paralogs (Philippidou and Dasen, 2013) (Figures 2B–2D; Figure S2A) but did not significantly repress transcription of rostral *HOX* genes (Figure S2B) or disrupt the NMP state (Figure 2B). Moreover, premature GDF11 treatment (initiated after 1 day of FGF8b/CHIR) could induce *HOXD10* but at >100-fold lower expression compared to GDF11 treatment after 4 days of FGF8b/CHIR, indicating robust lumbosacral patterning requires prior activation of rostral *HOX* genes (Figure S2C). We were able to detect colinear transcription of 33 of the 39 *HOX* genes in hPSC-derived NMP cultures, excluding *HOXB3*, *HOXC12*, and the *HOX13* paralogs, over a time span consistent with posterior neural tube formation according to the Carnegie stages of human development (Figure S2A). Moreover, temporal *HOX* activation was also observed in NMPs derived from IMR90-4 iPSCs (Figure S2D), indicating these mechanisms translate to other hPSC lines. While we believe the lack of *HOXB3* detection was due to experimental or qPCR reagent error, our extensive literature search was unable to find definitive documentation of *HOXC12* or *HOX13* paralog expression in the posterior CNS (Dasen et al., 2005).

## RA Converts NMPs to Neuroectoderm

In vivo, regression of the stem zone along the primitive streak yields a rostral decline in FGF signaling that coincides with RA secretion from newly formed somites and PAX6 expression in the newly formed neural tube (Diez del Corral et al., 2003). This suggests that RA could induce a NMP-to-neuroectoderm fate switch. To test this in vitro, we exposed hPSC-derived NMPs to E6 medium containing RA, CHIR, or neither for 2 days. Cultures exposed to only E6 medium maintained SOX2 and Brachyury expression but gained minimal PAX6 (96% ± 4% $SOX2^+$, 15% ± 8% $PAX6^+$, 78% ± 16% $Brachyury^+$), while exposure to only CHIR induced a mesodermal fate shift as evidenced by SOX2 downregulation, no PAX6 induction, and uniform maintenance of Brachyury expression (50% ± 8% $SOX2^+$, 96% ± 1% $Brachyury^+$) (Figure 3A). However, when exposed to RA, the cells gained PAX6 expression along with SOX2 maintenance (98% ± 4% $SOX2^+$, 97% ± 3% $PAX6^+$) and Brachyury downregulation (43% ± 4%) indicating a neuroectodermal fate shift (Figure 3A). Moreover, transitioning to RA at any point during NMP propagation generated a highly pure (>83%) $PAX6^+/SOX2^+$ neuroepithelial culture, i.e., polarized N-cadherin, within 4 days (Figures 3B–3D). If GDF11 was added to facilitate lumbosacral patterning, PAX6 expression in response to RA was decreased in a dose-dependent manner (Figures S3A–S3C). The ability of GDF11 to control R/C patterning is mediated by signaling via ALK5 (Andersson et al., 2006) and activation of the SMAD2/3 complex (Liu, 2006). GDF11 has also been shown to activate SMAD1/5/8 in vitro (Liu, 2006), which contributes to dorsal patterning (Tozer et al., 2013). Since dorsomorphin selectively inhibits ALK2, ALK3, and ALK6, which blocks SMAD1/5/8 signaling (Yu et al., 2008), we hypothesized the addition of dorsomorphin should prevent acquisition of a dorsal phenotype without affecting R/C patterning. Indeed, the addition of dorsomorphin with GDF11 and throughout RA treatment was sufficient to recover PAX6 expression (83% ± 4% $PAX6^+$; Figure S3D). Thus, highly pure neuroectoderm cultures could be obtained from NMPs at any point during colinear *HOX* activation.

## Deterministic Hox Patterning Can Be Achieved Using a Temporal Transition between Wnt/FGF/GDF and RA Treatment

Because RA production in vivo and treatment in vitro coincides with neural differentiation, we and others (Diez del Corral and Storey, 2004) posited that it might also serve as a signal to arrest colinear *HOX* activation. We therefore tested the ability of RA to generate neuroectoderm with discrete, region-specific *HOX* expression profiles in accordance with the status of colinear *HOX* activation observed in the NMP state (Figure 3B). Also, we assessed the expression of HOX transcription factors (TFs) that would demarcate distinct hindbrain and spinal cord domains (Dasen et al., 2003, 2005). First, we evaluated our ability to pattern neuroectoderm to hindbrain domains using a 0- to 30-hr FGF8b/CHIR NMP propagation period prior to 4 days of RA treatment (Figures 3B and 3C). qPCR analysis of the resulting neuroectoderm cultures revealed elevated expression of *HOXA1* and *HOXA2* prior to *HOXB1*, *HOXB2*, and *HOXB4*. Immunocytochemical analysis revealed that early cultures were $HOXB1^+/HOXB4^-$ (2 hr FGF8b/CHIR, 4 days RA; 63% ± 6% $HOXB1^+$) but rapidly lost HOXB1 expression if derived after only an additional 4 hr of NMP propagation (6 hr FGF8b/CHIR, 4 days RA; 5% ± 2% $HOXB1^+$) (Figure 3C). If neuroectoderm was derived after 24 hr of NMP propagation, it reacquired HOXB1 and now also expressed HOXB4 (24 hr FGF8b/CHIR, 4 days RA; 63% ± 5% $HOXB1^+$ and 37% ± 8% $HOXB4^+$) (Figure 3C). This mirrors HOX TF expression during development of the fourth, fifth, and sixth through eighth rhombomeres, respectively, indicating that transitioning from Wnt/FGF to RA at the 2- to 4-hr time point generates $HOXB1^+$ neuroectoderm that could potentially produce facial nerve MNs whereas

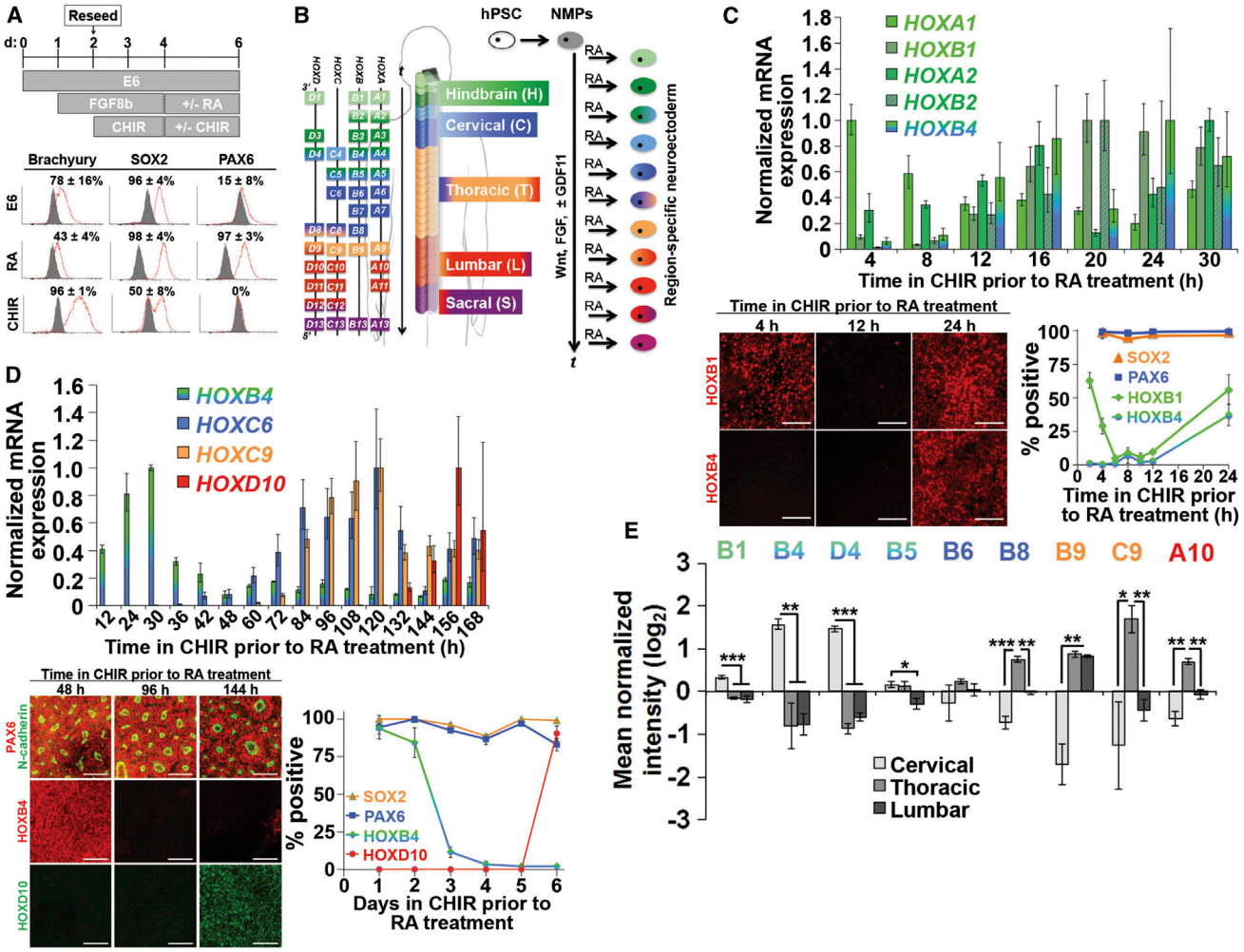


**Figure 3. RA Induces a Neuroectodermal Fate and Halts Colinear *HOX* Activation**

(A) NMPs exposed to RA or CHIR acquire a neuroectodermal or mesodermal fate as assessed by flow cytometry at day 6 (gray histogram, IgG control; red histogram, antigen of interest).

(B) Schematic for transition from NMPs to neuroectoderm by RA treatment. "t" indicates time under Wnt, FGF, and GDF signaling prior to RA treatment, which halts *HOX* progression to yield a defined rostrocaudal identity.

(C and D) Representative hindbrain (C) and spinal cord (D) cultures assessed by qPCR, immunocytochemistry, and flow cytometry. For all plots, flow cytometry data are presented as mean ± SD from biological duplicates, and qPCR data are mean ± SD from technical duplicates normalized to the time point of maximum expression for each gene. For hindbrain cultures, HOXB1 and HOXB4 were quantified by immunocytochemistry relative to $DAPI^+$ nuclei (technical triplicates per time point, minimum 10,000 cells counted, and relative HOX expression patterns were qualitatively verified across biological duplicates), while SOX2 and PAX6 were quantified by flow cytometry. For spinal cord cultures, HOXD10 was quantified by immunocytochemistry relative to $DAPI^+$ nuclei (technical duplicates, >2,000 cells counted), while SOX2, PAX6, and HOXB4 were quantified by flow cytometry. Scale bars, 100 μm. For (D), dorsomorphin was included with GDF11 and throughout RA treatment (further details in Figure S3).

(E) Mass spectrometry comparison of HOX profiles in cervical, thoracic, and lumbar neuroectoderm cultures. Cervical differentiation: 1 day FGF8b, 2 days FGF8b/CHIR, 4 days RA; thoracic differentiation: 1 day FGF8b, 6 days FGF8b/CHIR, 4 days RA; lumbar differentiation: 1 day FGF8b, 4 days FGF8b/CHIR, 2 days FGF8b/CHIR/GDF11, 4 days RA. Biological triplicates (neuroepithelium isolated individually from three separate culture wells) were used to calculate statistical significance between cervical, thoracic, and lumbar samples.

Data are presented as mean ± SD and statistical significance was calculated using the Student's unpaired t test. *$p < 0.01$; **$p < 0.002$; ***$p < 0.0001$.

transitioning at 24 hr generates HOXB4$^+$ neuroectoderm of the caudal hindbrain (Bell et al., 1999; Philippidou and Dasen, 2013; Bel-Vialar et al., 2002). Interestingly, the high percentage of HOXB1$^+$ cells at the 2 hr mark coincided with low *HOXB1* expression (~10% of the maximum observed expression at 20 hr) suggesting that while transcript levels are useful for identifying relative *HOX* gene expression, they may not be directly instructive for predicting HOX TF profiles that arise due to cross-repressive interactions (Bell et al., 1999; Dasen et al., 2003, 2005). Also, the observed abrupt transitions in neuroectoderm HOX TF expression suggest fairly uniform progressive *HOX* activation within the NMPs (Figure 3C).

Next, we performed a similar Wnt/FGF/GDF-to-RA transition time-course analysis focusing on later time points that would generate neuroectoderm patterned to spinal cord domains (Figures 3B and 3D). qPCR analysis again demonstrated that RA treatment could halt the induction of 5′ paralogs that would otherwise have become expressed in continuous Wnt/FGF/GDF11 treatment. Using both immunocytochemistry and flow cytometry, we observed uniform HOXB4 expression in neuroectodermal cultures derived from NMPs transitioned to RA after 24–48 hr of propagation, correlating to a rostral cervical spinal cord domain (Figures 3B and 3D). HOXB4 expression dropped sharply (from 84% ± 10% down to 12% ± 4% HOXB4$^+$ cells) when the transition to RA occurred at 72 hr (Figure 3D), which coincided with the initiation of thoracic *HOXC9* expression, a known repressor of *HOX4* paralog expression (Jung et al., 2010). Furthermore, HOXD10 was only detected in neuroectodermal cultures when RA was added after ~144 hr of NMP propagation (Figures 3B and 3D; Figure S3E), while HOXB4 remained repressed. Additional insights into the diversity of HOX expression in neuroectoderm patterned to cervical, thoracic, and lumbar spinal cord domains were obtained using quantitative mass spectrometry (Figure 3E; Table S1). As expected, HOXC9 was expressed in thoracic neuroectoderm but repressed in the HOXD10$^+$ lumbar culture, and many (HOXB1, HOXB4, HOXD4, HOXB5, HOXB8, HOXC9, and HOXA10) but not all (HOXB9) detected HOX factors exhibited expression patterns indicative of similar cross-repressive interactions (Dasen et al., 2005) (Figure 3E). Thus, these results demonstrate region-specific patterning of hPSC-derived neuroectoderm in the spinal cord, and similar to the hindbrain neuroectoderm cultures, repression of HOX proteins occurred even though their *HOX* transcripts remained expressed, possibly indicating cross-repressive interactions at this stage are occurring at the post-transcriptional stage (Yekta et al., 2004). Hence, our temporal biphasic approach for differentiating hPSCs to neuroectoderm through a stable NMP intermediate enables deterministic *HOX* patterning to impart diverse and discrete hindbrain and spinal cord regional identities (Figure 3B).

## Neuroectoderm with Region-Specific *HOX* Profiles Generate Regional MN Populations

We used MN differentiation to evaluate whether the regional specification imparted by our *HOX* patterning approach yielded characteristic differences in the neuroectoderm progeny. First, we verified that MNs derived from neuroectoderm of discrete hindbrain domains likewise exhibited distinct HOX signatures. Hindbrain neuromesoderm was propagated for 4, 12, and 24 hr before conversion to ventralized neuroectoderm using RA, sonic hedgehog (SHH) and purmorphamine (PM, a sonic hedgehog agonist) exposure and further differentiation to MNs using media containing RA and neurotrophic factors (NTFs). MN differentiation was verified by the presence of cells co-expressing βIII-tubulin/ISL1 and SMI-32 reactive non-phosphorylated neurofilament heavy chain with ISL1 or synapsin (Amoroso et al., 2013; Li et al., 2005) (Figure 4A). Immunocytochemical analysis of HB9$^+$ MNs generated from 4 hr neuromesoderm revealed no co-expression of HOXB1 or HOXB4. However, HB9$^+$ MNs generated from 12 hr neuromesoderm predominantly co-expressed HOXB1 but not HOXB4, and those generated from 24 hr neuromesoderm predominantly co-expressed both HOXB1 and HOXB4 (Figure 4A). Also, within all cultures, many ISL1$^+$ cells co-expressed PHOX2B indicative of hindbrain identity (Maury et al., 2014; Pattyn et al., 2000). Thus, MNs derived from hindbrain neuroectoderm with discrete Hox gene and protein profiles (Figure 3C) likewise express distinct HOX profiles, although the precise regional identity of these MNs based on their HOX signatures is currently unclear.

In the developed spinal cord, MNs reside in distinct motor columns: the lateral (LMC) and medial motor columns (MMC) at cervical and lumbar levels, and the preganglionic (PGC), MMC, and hypaxial motor column (HMC) at thoracic levels (Philippidou and Dasen, 2013). MMC MNs exclusively express LHX3 along with HB9 and ISL1, while LMC MNs express LHX1 and FOXP1 with either HB9 or ISL1 depending on their further subdivision into medial and lateral domains (Thaler et al., 1999; Tsuchida et al., 1994). PGC MNs are FOXP1$^+$/ISL1$^+$/HB9$^-$, while HMC MNs are LHX3$^-$/FOXP1$^-$ but express both HB9 and ISL1 (Dasen et al., 2008; William et al., 2003). Thus, quantitative immunocytochemistry can be used to observe whether cervical, thoracic, and lumbar neuroectoderm could be differentiated into MN precursors populations exhibiting relative FOXP1/HB9 co-expression patterns characteristic of their R/C domain in vivo, i.e., the presence of FOXP1$^+$/HB9$^+$ cells in cervical and lumbar but not thoracic cultures (Dasen et al., 2008).

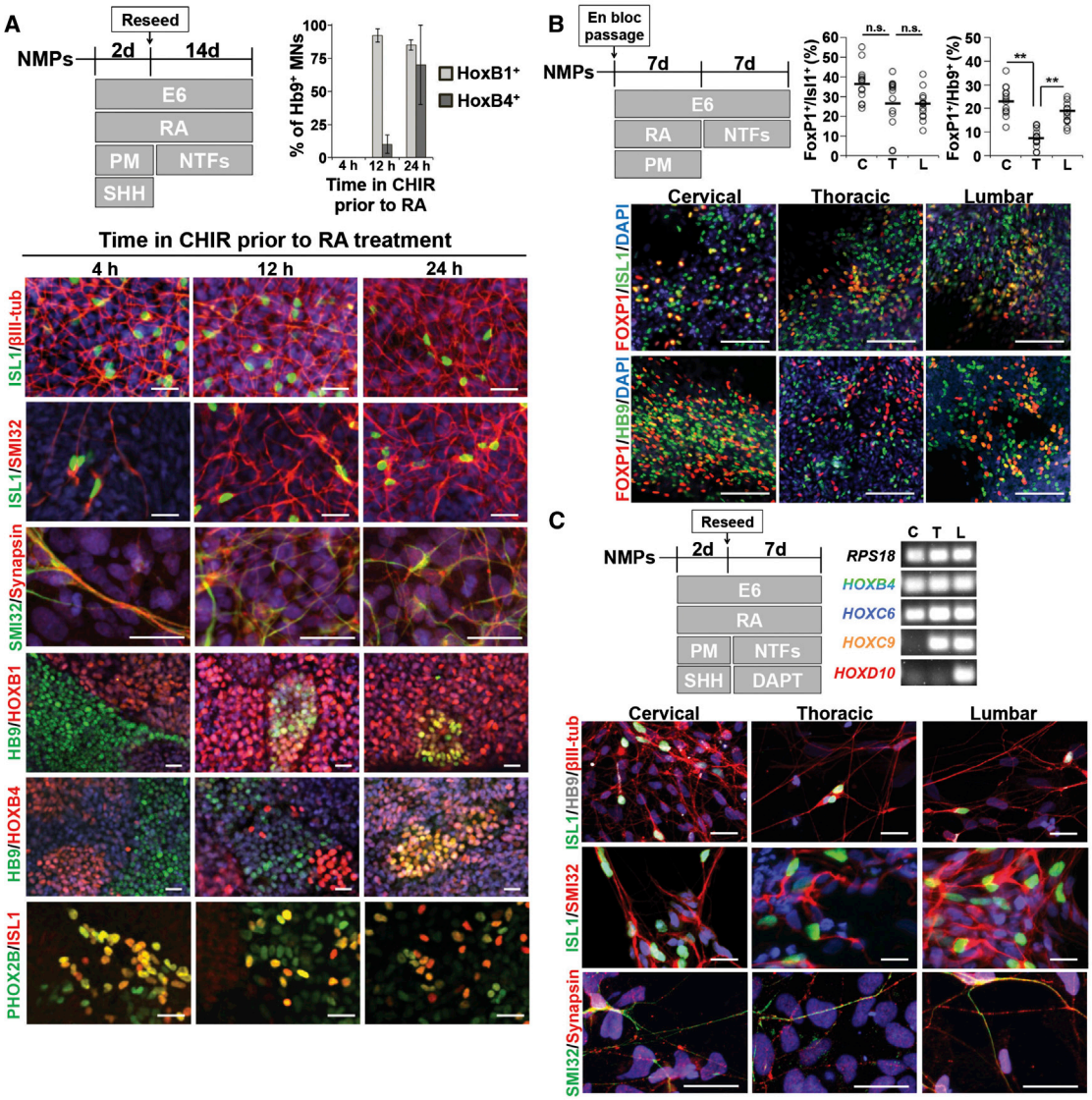


**Figure 4. Derivation of Region-Specific MNs**

(A) Neuronal maturation from various hindbrain locales. NMPs were propagated for 4, 12, or 24 hr before conversion to ventralized neuroectoderm and differentiation to neurons. DAPI (blue) is overlaid in most images. Scale bars, 20 μm. Quantified data are presented as mean ± SD (four technical replicates, >100 $HB9^+$ cells counted per sample).

(B) Evaluation of FOXP1 columnar identity in $ISL1^+$ and $HB9^+$ MNs. Cervical differentiation (C): 1 day FGF8b, 2 days FGF8b/CHIR; thoracic differentiation (T): 1 day FGF8b, 5 days FGF8b/CHIR; lumbar differentiation (L): 1 day FGF8b, 4 days FGF8b/CHIR, 2 days FGF8b/CHIR/GDF11; prior to en bloc passage and further differentiation as indicated. NTFs, neurotrophic factors (described in Experimental Procedures). For plotted data, open circles are percentages from individual fields and bars indicate the mean. Statistical significance was calculated using the Student's unpaired t test (three to five fields were counted across three biological replicates for each condition, minimum 2,500 cells counted). n.s., $p > 0.02$; **$p < 0.000001$. Scale bars, 100 μm.

(C) Neuronal maturation from cervical, thoracic, and lumbar patterned neuroectoderm corresponding to the NMP state described in (B). DAPI is overlaid in all images. Scale bars, 20 μm. RT-PCR (50 cycles) demonstrates maintenance of regional identity.

Regional spinal MN precursors were derived by exposing appropriately patterned NMPs to RA and PM for 7 days prior to an additional week of differentiation in neurotrophic factors (Li et al., 2005) (Figure 4B). We observed no significant differences in the numbers of $FOXP1^+$/$ISL1^+$ MN precursors (37% ± 9%, 27% ± 13%, and 26% ± 8%, respectively, of the total $ISL1^+$ population). However, $FOXP1^+$/$HB9^+$ MN precursors were prevalent in cervical

and lumbar cultures (23% ± 6% and 18% ± 4% of the total HB9$^+$ population) but scarce in thoracic cultures (8% ± 4%; $p < 0.000001$, Figure 4B). We initially expected that no FOXP1$^+$/HB9$^+$ MN precursors would be present in the thoracic cultures, but PGC MNs proceed through an HB9$^+$ state before its expression is rapidly lost (William et al., 2003). Therefore, the small subset of FOXP1$^+$/HB9$^+$ cells in our thoracic cultures likely represents immature PGC MNs. The significant difference in the propensity of cervical and lumbar versus thoracic neuroectoderm to generate FOXP1$^+$/HB9$^+$ MN precursors characteristic of the LMC demonstrates proper regional specification as a result of our deterministic *HOX* patterning approach.

Furthermore, we investigated whether accelerated MN differentiation induced by treating ventralized cervical (*HOXC6*$^+$/*HOXC9*$^-$/*HOXD10*$^-$), thoracic (*HOXC6*$^+$/*HOXC9*$^+$/*HOXD10*$^-$), and lumbar (*HOXC6*$^+$/*HOXC9*$^+$/*HOXD10*$^+$) (Figure 3D) neuroectoderm with the Notch signaling inhibitor DAPT (Maury et al., 2014), which yielded >92% NeuN$^+$ neuronal cultures within 7 days (Figures 4C and S4A), altered the regional specification imposed at the neuroectoderm stage. Each differentiated culture contained MNs co-expressing βIII-tubulin with ISL1 or HB9 and SMI-32 with ISL1 or synapsin (Figure 4C). RT-PCR analysis revealed that each culture's regional spinal cord identity patterned at the neuroectodermal state was preserved throughout accelerated neuronal differentiation (Figure 4C). Also, electrophysiological analysis of these cervical, thoracic, and lumbar cultures after additional weeks of maturation determined that each region-specific culture possessed neurons exhibiting mature action potentials (Figures S4B and S4C). Hence, our approach to deterministic patterning of *HOX* expression should be broadly applicable to deriving functional and region-specific hindbrain and spinal cord tissues from hPSCs.

## DISCUSSION

### Regulation of *HOX* Expression during Posterior Neural Differentiation of hPSCs

Our results provide unique evidence that *HOX* expression during posterior neural differentiation of hPSCs can be precisely regulated by temporal control of two opposing mechanisms. Wnt/β-catenin, FGF, and GDF signaling synergistically control colinear *HOX* activation while maintaining an NMP state, and RA arrests *HOX* activation to yield a fixed R/C position and transitions the cultures to definitive neuroectoderm. This approach should enable the derivation of neuroectoderm from any R/C position spanning the hindbrain to lumbosacral spinal cord in a predictable manner.

Specifically, we have demonstrated the ability to generate neuroectoderm with HOX profiles corresponding to specific rhombomeric segments and cervical, thoracic, and lumbosacral vertebral segments. Our findings are distinct from other PSC neural differentiation approaches that unpredictably pattern cells to primarily caudal hindbrain thru cervical *HOX* profiles (Amoroso et al., 2013; Lee et al., 2007; Li et al., 2005) or to heterogeneous mixtures of cervical, thoracic, and lumbar tissues (Patani et al., 2011; Peljto et al., 2010). Given the data presented in our manuscript, it is perhaps surprising that RA-only patterning approaches can yield *HOX6-8* expression, but this may be inherent to the choice of differentiation methods. Whereas we utilized a chemically defined monolayer system to screen *HOX* patterning cues, most other studies have used embryoid body (EB) cultures for posterior neural differentiation. EB differentiation has been shown to activate endogenous Wnt signaling (Li et al., 2009), but cells in outer layers of EBs are exposed to different concentrations of soluble media cues than those on the inside of EBs due to diffusional limitations (Van Winkle et al., 2012). Therefore, we suspect in these EB-based systems that competition between endogenous Wnt (activating *HOX* progression) and exogenously added RA (inducing *HOX* arrest and neural differentiation) could cause heterogeneous R/C patterning, especially when considering relative heterogeneity in EB sizes and shapes. In contrast, exposure to soluble factors in our monolayer differentiation system should be more uniform, possibly enabling our enhanced *HOX* patterning precision.

We also provide evidence that Wnt/β-catenin and FGF signaling alone can induce substantial expression of *CDX* genes, which are core regulators of *HOX* expression in vivo, similar to results from tissue explant and other PSC differentiation studies (Gouti et al., 2014; Maury et al., 2014; Mazzoni et al., 2013; Nordström et al., 2006). Thus, RA and Wnt/FGF signaling may regulate different epigenetic states, which could potentially explain discrepancies between reports of coarse, saltatory *HOX* activation in vitro by RA alone (Mazzoni et al., 2013) versus the induction of organized, colinear *HOX* activation in vivo by the temporal integration of multiple signaling pathways. Moreover, though previous studies have suggested RA serves as a "rostralizing" factor (Philippidou and Dasen, 2013), our treatment of thoracic or lumbosacral NMPs with RA did not generate rostralized neuroectoderm (Figure 3D); as such, we postulate these previous studies were actually observing premature termination of *HOX* progression. From our results, we posit that *HOX* patterning may involve a temporal, biphasic mechanism where Wnt/FGF primarily controls colinear *HOX* activation and RA controls its termination. This is different than the widely cited gradient mechanism that supposes RA controls 3′ *HOX*

patterning and Wnt/FGF controls 5′ *HOX* patterning (Philippidou and Dasen, 2013). Our patterning mechanism resonates with a progress/stem zone model that has been heavily scrutinized for limb development (Towers and Tickle, 2009). However, our in vitro approach does not allow us to draw direct conclusions about the role each of these factors plays in *HOX* regulation in vivo. We are instead hopeful that our patterning approach will enable detailed studies of *HOX* regulation in vitro, which could then be used to conduct more informative studies of *HOX* patterning in vivo. In addition, since much of the "Hoxasome" is still poorly understood (Mann et al., 2009), the scalability of our chemically defined, deterministic *HOX* patterning protocol will be invaluable to elucidating the molecular mechanisms underlying Hox regulation of downstream neural cell fates.

### Implications for Regenerative Therapies and Disease Modeling

Recent studies of cell replacement therapy in the anterior CNS using hPSC-derived progenitors have demonstrated that the implanted cells must possess a regional phenotype that mimics endogenous tissues in order to effectively engraft and correct neural deficits (Kriks et al., 2011; Ma et al., 2012). Since *HOX* expression patterns are crucial determinants of cellular phenotype, organization, and neural circuit integration in the developing hindbrain and spinal cord (Philippidou and Dasen, 2013), our patterning approach could serve as the basis for generating a spectrum of posterior neural progeny with highly specific regional identities that may aid regenerative therapy efforts. Also, regional MN phenotypes exhibit differential susceptibility to several neurodegenerative disorders, including amyotrophic lateral sclerosis (ALS) and spinal muscular atrophy (SMA) (Brockington et al., 2013; Kaplan et al., 2014). Our deterministic *HOX* patterning approach will facilitate elucidation of the molecular basis underlying differential susceptibility of iPSC-derived MNs with the same disease-causing mutations but different regional phenotypes, including previously inaccessible hindbrain phenotypes. The ability to execute such experimental paradigms should significantly enhance the utility of iPSC-derived MN disease models to identify relevant pathways of neurodegenerative disease induction and progression (Chen et al., 2014; Kiskinis et al., 2014).

## EXPERIMENTAL PROCEDURES

### Induction and Propagation of NMPs and Differentiation to Neural Fates

H9 hESCs (Thomson et al., 1998) (passage 25–45), H9 ishcat2 hESCs (Lian et al., 2012) (passage 33–43), and IMR90-4 iPSCs (Yu et al., 2007) (passage 31–40) were maintained in E8 medium on Matrigel (BD Biosciences) as previously described (Lippmann et al., 2014). 2 μg/ml doxycycline (Sigma) was used for β-catenin knockdown in the ishcat2 line. To initiate differentiation, hPSCs were passaged with accutase (Life Technologies) onto vitronectin (VTN-NC)-coated (Chen et al., 2011) plates at a density of 1 × $10^5$ cells/$cm^2$ with 10 μM ROCK inhibitor (Y27632; R&D Systems) as previously described (Lippmann et al., 2014). The following day, cells were changed to E6 medium and then changed to E6 medium containing 200 ng/ml FGF8b 24 hr later (PeproTech). After another day, the cells were washed once with 2 ml PBS, accutased for 2 min, and removed from the surface by gentle pipetting. After collection by centrifugation, cells were gently resuspended in E6 medium containing 200 ng/ml FGF8b and CHIR99021 (CHIR, 3 μM for H9 hESCs and 2 μM for IMR90-4 iPSCs; R&D Systems) and re-seeded on VTN-NC-coated plates at a density of 1.5 × $10^5$ cells/$cm^2$. 10 μM Y27632 was included during the re-seeding process, and the medium was not changed again until 48 hr after passaging. If extended NMP propagation was required, this passaging process was repeated on day 3 of CHIR treatment (re-seed density of 1.2 × $10^5$ cells/$cm^2$), and 50 ng/ml GDF11 (PeproTech) was added on day 4 of CHIR treatment to initiate lumbosacral patterning. For some experiments, 1 μM dorsomorphin (R&D Systems) was included with GDF11. At any point during CHIR treatment, cells were changed to E6 medium containing 1 μM retinoic acid (RA; Sigma) to elicit neural induction and arrest *HOX* progression. For assessment of FOXP1 expression in MN precursors, NMPs were passaged en bloc by scraping and re-seeded in VTN-NC-coated chamber slides at a 1:200 ratio in E6 medium containing 1 μM RA and 100 nM purmorphamine (PM; Cayman Chemicals) for 7 days, followed by an additional 7-day treatment with 10 ng/ml brain-derived neurotrophic factor (BDNF; PeproTech), 10 ng/ml glial-derived neurotrophic factor (GDNF; PeproTech), and cAMP (1 μM; Sigma). For assessment of HOX identity in MNs, NMPs were neuralized and ventralized with 1 μM RA, 2 μM PM, and 1 μg/ml sonic hedgehog (SHH; R&D Systems) for 2 days and then passaged en bloc or with accutase and re-seeded in VTN-NC-coated chamber slides at 2 × $10^4$ cells/$cm^2$ in E6 medium containing RA, 10 μM Y27632, 10 ng/ml BDNF, 10 ng/ml GDNF, and 1 μM cAMP for 7–14 days (Y27632 was removed after the first 3 days). 10 nM RA was used for cultures with hindbrain *HOX* signatures, and 1 μM RA was used for cultures with spinal cord *HOX* signatures. 1 μM DAPT (Cayman Chemicals) was included for cultures with spinal cord identity. For extended neuronal differentiation to conduct electrophysiology studies, NMPs were neuralized and ventralized with 1 μM RA, 2 μM PM, and 1 μg/ml SHH, passaged 1:100 onto Matrigel-coated glass coverslips, and cultured for 7 days in E6 medium containing 1 μM RA, 100 nM PM, 100 ng/ml SHH, and 1 μM DAPT. The cultures were then matured in E6 medium containing 10 ng/ml BDNF, 10 ng/ml GDNF, and 1 μM cAMP for at least 2 months prior to electrophysiology measurements. The cells were supplemented with 1 μg/ml mouse laminin (Invitrogen) once per week to help maintain attachment.

## SUPPLEMENTAL INFORMATION

Supplemental Information includes Supplemental Experimental Procedures, four figures, and four tables and can be found

with this article online at http://dx.doi.org/10.1016/j.stemcr.2015.02.018.

## AUTHOR CONTRIBUTIONS

E.S.L. and R.S.A. conceived the study. E.S.L. and M.C.E.-S. performed all cell-culture experiments and related analyses. C.E.W. and J.J.C. designed the mass spectrometry proteomic analysis and C.E.W. conducted these experiments. D.A.R. and E.R.C. conducted and supervised the electrophysiology experiments, respectively. All authors contributed to manuscript preparation.

## ACKNOWLEDGMENTS

We would like to thank Dr. James Thomson and Nicholas Propson for providing the vitronectin peptide, Dr. Sean Palecek for providing the H9 ishcat2 line, and Dr. John Yin for use of the Biorad CFX96 qPCR machine. The PAX6, HOXB4, HB9, and ISL1 antibodies used in this study were obtained from the Developmental Studies Hybridoma Bank developed under the auspices of the NICHD and maintained by the University of Iowa. The HOXD10 antibody was obtained as a pre-release reagent from R&D Systems. This work was supported by funding from the Wisconsin Institutes for Discovery (R.S.A.), a Draper Technology Innovation Fund Award from the Wisconsin Alumni Research Foundation (R.S.A.), and NIH grants R21 NS082618 (R.S.A.), R01 GM080148 (J.J.C.) and R01 MH061876 (E.R.C.). E.S.L. was supported by a postdoctoral fellowship from the University of Wisconsin Stem Cell and Regenerative Medicine Center (SCRMC) and an Individual Postdoctoral National Research Service Award (NRSA) from the NIH (1F32NS083291-01A1). D.A.R. was supported by a National Science Foundation (NSF) GRSP fellowship (DGE-1256259) and the Neuroscience Training Program (T32-GM007507). E.R.C. is an Investigator of the Howard Hughes Medical Institute. R.S.A. holds an Innovation in Regulatory Science Award for the Burroughs Wellcome Fund.

Received: January 16, 2015
Revised: February 23, 2015
Accepted: February 24, 2015
Published: April 2, 2015

## REFERENCES

Amoroso, M.W., Croft, G.F., Williams, D.J., O'Keeffe, S., Carrasco, M.A., Davis, A.R., Roybon, L., Oakley, D.H., Maniatis, T., Henderson, C.E., and Wichterle, H. (2013). Accelerated high-yield generation of limb-innervating motor neurons from human stem cells. J. Neurosci. *33*, 574–586.

Andersson, O., Reissmann, E., and Ibáñez, C.F. (2006). Growth differentiation factor 11 signals through the transforming growth factor-β receptor ALK5 to regionalize the anterior-posterior axis. EMBO Rep. *7*, 831–837.

Bel-Vialar, S., Itasaki, N., and Krumlauf, R. (2002). Initiating Hox gene expression: in the early chick neural tube differential sensitivity to FGF and RA signaling subdivides the HoxB genes in two distinct groups. Development *129*, 5103–5115.

Bell, E., Wingate, R.J.T., and Lumsden, A. (1999). Homeotic transformation of rhombomere identity after localized Hoxb1 misexpression. Science *284*, 2168–2171.

Bertrand, N., Médevielle, F., and Pituello, F. (2000). FGF signalling controls the timing of Pax6 activation in the neural tube. Development *127*, 4837–4843.

Brockington, A., Ning, K., Heath, P.R., Wood, E., Kirby, J., Fusi, N., Lawrence, N., Wharton, S.B., Ince, P.G., and Shaw, P.J. (2013). Unravelling the enigma of selective vulnerability in neurodegeneration: motor neurons resistant to degeneration in ALS show distinct gene expression characteristics and decreased susceptibility to excitotoxicity. Acta Neuropathol. *125*, 95–109.

Chen, G., Gulbranson, D.R., Hou, Z., Bolin, J.M., Ruotti, V., Probasco, M.D., Smuga-Otto, K., Howden, S.E., Diol, N.R., Propson, N.E., et al. (2011). Chemically defined conditions for human iPSC derivation and culture. Nat. Methods *8*, 424–429.

Chen, H., Qian, K., Du, Z., Cao, J., Petersen, A., Liu, H., Blackbourn, L.W., 4th, Huang, C.-L., Errigo, A., Yin, Y., et al. (2014). Modeling ALS with iPSCs reveals that mutant SOD1 misregulates neurofilament balance in motor neurons. Cell Stem Cell *14*, 796–809.

Dasen, J.S., Liu, J.-P., and Jessell, T.M. (2003). Motor neuron columnar fate imposed by sequential phases of Hox-c activity. Nature *425*, 926–933.

Dasen, J.S., Tice, B.C., Brenner-Morton, S., and Jessell, T.M. (2005). A Hox regulatory network establishes motor neuron pool identity and target-muscle connectivity. Cell *123*, 477–491.

Dasen, J.S., De Camilli, A., Wang, B., Tucker, P.W., and Jessell, T.M. (2008). Hox repertoires for motor neuron diversity and connectivity gated by a single accessory factor, FoxP1. Cell *134*, 304–316.

Delfino-Machín, M., Lunn, J.S., Breitkreuz, D.N., Akai, J., and Storey, K.G. (2005). Specification and maintenance of the spinal cord stem zone. Development *132*, 4273–4283.

Diez del Corral, R., and Storey, K.G. (2004). Opposing FGF and retinoid pathways: a signalling switch that controls differentiation and patterning onset in the extending vertebrate body axis. BioEssays *26*, 857–869.

Diez del Corral, R., Olivera-Martinez, I., Goriely, A., Gale, E., Maden, M., and Storey, K. (2003). Opposing FGF and retinoid pathways control ventral neural pattern, neuronal differentiation, and segmentation during body axis extension. Neuron *40*, 65–79.

Gould, A., Itasaki, N., and Krumlauf, R. (1998). Initiation of rhombomeric Hoxb4 expression requires induction by somites and a retinoid pathway. Neuron *21*, 39–51.

Gouti, M., Tsakiridis, A., Wymeersch, F.J., Huang, Y., Kleinjung, J., Wilson, V., and Briscoe, J. (2014). In vitro generation of neuromesodermal progenitors reveals distinct roles for wnt signalling in the specification of spinal cord and paraxial mesoderm identity. PLoS Biol. *12*, e1001937.

Iimura, T., and Pourquié, O. (2006). Collinear activation of Hoxb genes during gastrulation is linked to mesoderm cell ingression. Nature *442*, 568–571.

Jung, H., Lacombe, J., Mazzoni, E.O., Liem, K.F., Jr., Grinstein, J., Mahony, S., Mukhopadhyay, D., Gifford, D.K., Young, R.A., Anderson, K.V., et al. (2010). Global control of motor neuron topography

mediated by the repressive actions of a single hox gene. Neuron *67*, 781–796.

Kaplan, A., Spiller, K.J., Towne, C., Kanning, K.C., Choe, G.T., Geber, A., Akay, T., Aebischer, P., and Henderson, C.E. (2014). Neuronal matrix metalloproteinase-9 is a determinant of selective neurodegeneration. Neuron *81*, 333–348.

Kiskinis, E., Sandoe, J., Williams, L.A., Boulting, G.L., Moccia, R., Wainger, B.J., Han, S., Peng, T., Thams, S., Mikkilineni, S., et al. (2014). Pathways disrupted in human ALS motor neurons identified through genetic correction of mutant SOD1. Cell Stem Cell *14*, 781–795.

Krencik, R., Weick, J.P., Liu, Y., Zhang, Z.-J., and Zhang, S.-C. (2011). Specification of transplantable astroglial subtypes from human pluripotent stem cells. Nat. Biotechnol. *29*, 528–534.

Kriks, S., Shim, J.-W., Piao, J., Ganat, Y.M., Wakeman, D.R., Xie, Z., Carrillo-Reid, L., Auyeung, G., Antonacci, C., Buch, A., et al. (2011). Dopamine neurons derived from human ES cells efficiently engraft in animal models of Parkinson's disease. Nature *480*, 547–551.

Lee, H., Shamy, G.A., Elkabetz, Y., Schofield, C.M., Harrsion, N.L., Panagiotakos, G., Socci, N.D., Tabar, V., and Studer, L. (2007). Directed differentiation and transplantation of human embryonic stem cell-derived motoneurons. Stem Cells *25*, 1931–1939.

Lewis, E.B. (1978). A gene complex controlling segmentation in Drosophila. Nature *276*, 565–570.

Li, X.-J., Du, Z.-W., Zarnowska, E.D., Pankratz, M., Hansen, L.O., Pearce, R.A., and Zhang, S.-C. (2005). Specification of motoneurons from human embryonic stem cells. Nat. Biotechnol. *23*, 215–221.

Li, X.-J., Hu, B.-Y., Jones, S.A., Zhang, Y.-S., Lavaute, T., Du, Z.-W., and Zhang, S.-C. (2008). Directed differentiation of ventral spinal progenitors and motor neurons from human embryonic stem cells by small molecules. Stem Cells *26*, 886–893.

Li, X.-J., Zhang, X., Johnson, M.A., Wang, Z.-B., Lavaute, T., and Zhang, S.-C. (2009). Coordination of sonic hedgehog and Wnt signaling determines ventral and dorsal telencephalic neuron types from human embryonic stem cells. Development *136*, 4055–4063.

Lian, X., Hsiao, C., Wilson, G., Zhu, K., Hazeltine, L.B., Azarin, S.M., Raval, K.K., Zhang, J., Kamp, T.J., and Palecek, S.P. (2012). Robust cardiomyocyte differentiation from human pluripotent stem cells via temporal modulation of canonical Wnt signaling. Proc. Natl. Acad. Sci. USA *109*, E1848–E1857.

Lippmann, E.S., Estevez-Silva, M.C., and Ashton, R.S. (2014). Defined human pluripotent stem cell culture enables highly efficient neuroepithelium derivation without small molecule inhibitors. Stem Cells *32*, 1032–1042.

Liu, J.-P. (2006). The function of growth/differentiation factor 11 (Gdf11) in rostrocaudal patterning of the developing spinal cord. Development *133*, 2865–2874.

Liu, J.-P., Laufer, E., and Jessell, T.M. (2001). Assigning the positional identity of spinal motor neurons: rostrocaudal patterning of Hox-c expression by FGFs, Gdf11, and retinoids. Neuron *32*, 997–1012.

Ma, L., Hu, B., Liu, Y., Vermilyea, S.C., Liu, H., Gao, L., Sun, Y., Zhang, X., and Zhang, S.-C. (2012). Human embryonic stem cell-derived GABA neurons correct locomotion deficits in quinolinic acid-lesioned mice. Cell Stem Cell *10*, 455–464.

Mann, R.S., Lelli, K.M., and Joshi, R. (2009). Hox specificity: unique roles for cofactors and collaborators. In Current Topics in Developmental Biology, Chapter 3, O. Pourquié, ed. (2009). (Academic Press), pp. 63–101.

Mathis, L., Kulesa, P.M., and Fraser, S.E. (2001). FGF receptor signalling is required to maintain neural progenitors during Hensen's node progression. Nat. Cell Biol. *3*, 559–566.

Maury, Y., Côme, J., Piskorowski, R.A., Salah-Mohellibi, N., Chevaleyre, V., Peschanski, M., Martinat, C., and Nedelec, S. (2014). Combinatorial analysis of developmental cues efficiently converts human pluripotent stem cells into multiple neuronal subtypes. Nat. Biotechnol.

Mazzoni, E.O., Mahony, S., Peljto, M., Patel, T., Thornton, S.R., McCuine, S., Reeder, C., Boyer, L.A., Young, R.A., Gifford, D.K., and Wichterle, H. (2013). Saltatory remodeling of Hox chromatin in response to rostrocaudal patterning signals. Nat. Neurosci. *16*, 1191–1198.

Molotkova, N., Molotkov, A., Sirbu, I.O., and Duester, G. (2005). Requirement of mesodermal retinoic acid generated by Raldh2 for posterior neural transformation. Mech. Dev. *122*, 145–155.

Nordström, U., Maier, E., Jessell, T.M., and Edlund, T. (2006). An early role for WNT signaling in specifying neural patterns of Cdx and Hox gene expression and motor neuron subtype identity. PLoS Biol. *4*, e252.

Patani, R., Hollins, A.J., Wishart, T.M., Puddifoot, C.A., Álvarez, S., de Lera, A.R., Wyllie, D.J.A., Compston, D.A., Pedersen, R.A., Gillingwater, T.H., et al. (2011). Retinoid-independent motor neurogenesis from human embryonic stem cells reveals a medial columnar ground state. Nat. Commun. *2*, 214.

Pattyn, A., Hirsch, M., Goridis, C., and Brunet, J.F. (2000). Control of hindbrain motor neuron differentiation by the homeobox gene Phox2b. Development *127*, 1349–1358.

Peljto, M., Dasen, J.S., Mazzoni, E.O., Jessell, T.M., and Wichterle, H. (2010). Functional diversity of ESC-derived motor neuron subtypes revealed through intraspinal transplantation. Cell Stem Cell *7*, 355–366.

Philippidou, P., and Dasen, J.S. (2013). Hox genes: choreographers in neural development, architects of circuit organization. Neuron *80*, 12–34.

Sandoe, J., and Eggan, K. (2013). Opportunities and challenges of pluripotent stem cell neurodegenerative disease models. Nat. Neurosci. *16*, 780–789.

Takemoto, T., Uchikawa, M., Kamachi, Y., and Kondoh, H. (2006). Convergence of Wnt and FGF signals in the genesis of posterior neural plate through activation of the Sox2 enhancer N-1. Development *133*, 297–306.

Takemoto, T., Uchikawa, M., Yoshida, M., Bell, D.M., Lovell-Badge, R., Papaioannou, V.E., and Kondoh, H. (2011). Tbx6-dependent Sox2 regulation determines neural or mesodermal fate in axial stem cells. Nature *470*, 394–398.

Thaler, J., Harrison, K., Sharma, K., Lettieri, K., Kehrl, J., and Pfaff, S.L. (1999). Active suppression of interneuron programs within developing motor neurons revealed by analysis of homeodomain factor HB9. Neuron *23*, 675–687.

Thomson, J.A., Itskovitz-Eldor, J., Shapiro, S.S., Waknitz, M.A., Swiergiel, J.J., Marshall, V.S., and Jones, J.M. (1998). Embryonic stem cell lines derived from human blastocysts. Science *282*, 1145–1147.

Towers, M., and Tickle, C. (2009). Growing models of vertebrate limb development. Development *136*, 179–190.

Tozer, S., Le Dréau, G., Marti, E., and Briscoe, J. (2013). Temporal control of BMP signalling determines neuronal subtype identity in the dorsal neural tube. Development *140*, 1467–1474.

Tsuchida, T., Ensini, M., Morton, S.B., Baldassare, M., Edlund, T., Jessell, T.M., and Pfaff, S.L. (1994). Topographic organization of embryonic motor neurons defined by expression of LIM homeobox genes. Cell *79*, 957–970.

Tzouanacou, E., Wegener, A., Wymeersch, F.J., Wilson, V., and Nicolas, J.-F. (2009). Redefining the progression of lineage segregations during mammalian embryogenesis by clonal analysis. Dev. Cell *17*, 365–376.

Van Winkle, A.P., Gates, I.D., and Kallos, M.S. (2012). Mass transfer limitations in embryoid bodies during human embryonic stem cell differentiation. Cells Tissues Organs (Print) *196*, 34–47.

Wichterle, H., Lieberam, I., Porter, J.A., and Jessell, T.M. (2002). Directed differentiation of embryonic stem cells into motor neurons. Cell *110*, 385–397.

William, C.M., Tanabe, Y., and Jessell, T.M. (2003). Regulation of motor neuron subtype identity by repressor activity of Mnx class homeodomain proteins. Development *130*, 1523–1536.

Yekta, S., Shih, I.H., and Bartel, D.P. (2004). MicroRNA-directed cleavage of HOXB8 mRNA. Science *304*, 594–596.

Yu, J., Vodyanik, M.A., Smuga-Otto, K., Antosiewicz-Bourget, J., Frane, J.L., Tian, S., Nie, J., Jonsdottir, G.A., Ruotti, V., Stewart, R., et al. (2007). Induced pluripotent stem cell lines derived from human somatic cells. Science *318*, 1917–1920.

Yu, P.B., Hong, C.C., Sachidanandan, C., Babitt, J.L., Deng, D.Y., Hoyng, S.A., Lin, H.Y., Bloch, K.D., and Peterson, R.T. (2008). Dorsomorphin inhibits BMP signals required for embryogenesis and iron metabolism. Nat. Chem. Biol. *4*, 33–41.

**Stem Cell Reports, Volume *4***

**Supplemental Information**

# Deterministic *HOX* Patterning in Human Pluripotent Stem Cell-Derived Neuroectoderm

**Ethan S. Lippmann, Clay E. Williams, David A. Ruhl, Maria C. Estevez-Silva, Edwin R. Chapman, Joshua J. Coon, and Randolph S. Ashton**

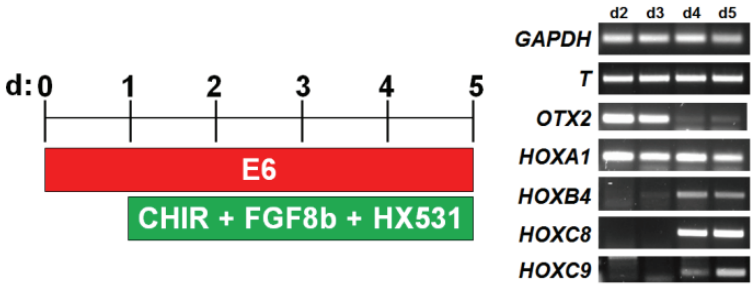


**Figure S1. Inhibition of RA signaling by 1 μM HX531 does not disrupt *HOX* progression, related to Figure 1**. RT-PCR data indicates that CHIR/FGF8b effects are not indirectly mediated by endogenous RA signaling.

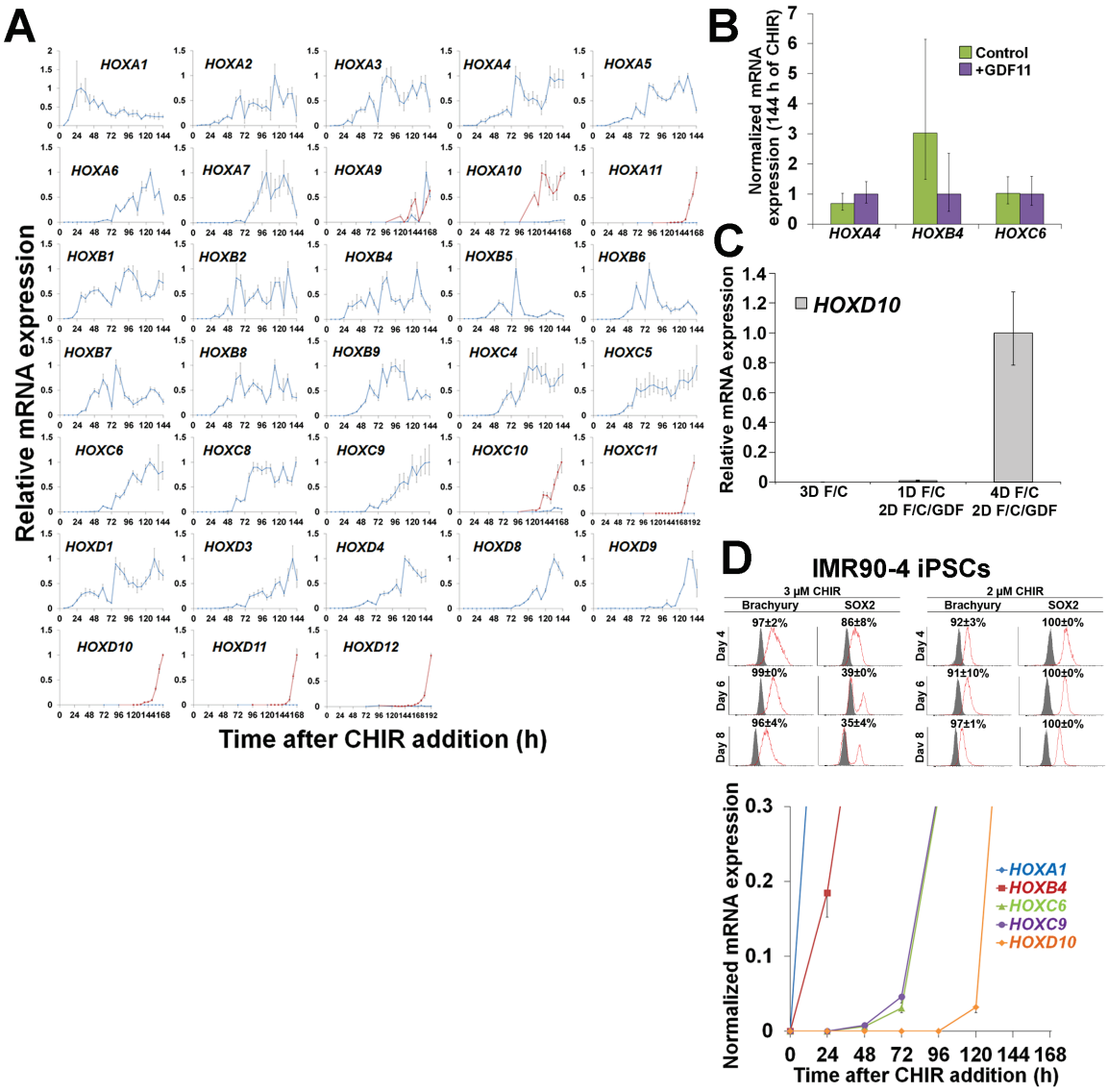


**Figure S2. *HOX* regulation in the neuromesodermal state, related to Figure 2. (A)** qPCR analysis of *HOX* expression during neuromesodermal propagation in H9 hESCs. Experimental timing is found in Figure 2B. Data are presented as mean ± S.D. from technical duplicates normalized to maximum expression for each gene. Blue lines = samples not receiving GDF11; red lines = samples receiving GDF11 according to Figure 2B. *HOXC11* and *HOXD12* required 192 h of CHIR treatment to be appreciably detected. **(B)** Rostral *HOX* expression is unaffected by GDF11 treatment during H9 hESC neuromesodermal propagation. qPCR data are presented as mean ± S.D. from technical duplicates normalized to the GDF11-treated sample for each

gene. **(C)** Premature treatment with GDF11 during neuromesodermal propagation does not effectively induce *HOXD10*. qPCR data are presented as mean ± S.D. from technical duplicates normalized to the condition of maximum *HOXD10* expression. **(D)** Evaluation of neuromesodermal propagation and *HOX* expression in IMR90-4 iPSCs. Differentiation was conducted according to Figure 2B. The neuromesodermal phenotype was assessed during differentiation in 2 or 3 μM CHIR. Grey histograms, IgG control. Red histograms, label of interest. Whereas 2 μM CHIR maintained the neuromesodermal state, 3 μM CHIR resulted in a mesodermal shift exemplified by a reduction in SOX2 expression. Data were collected by flow cytometry and presented as mean ± S.D. from biological duplicates. During neuromesodermal propagation, progressive *HOX* activation was also verified by qPCR. Data are presented as mean ± S.D. from technical duplicates normalized to maximum expression for each gene.

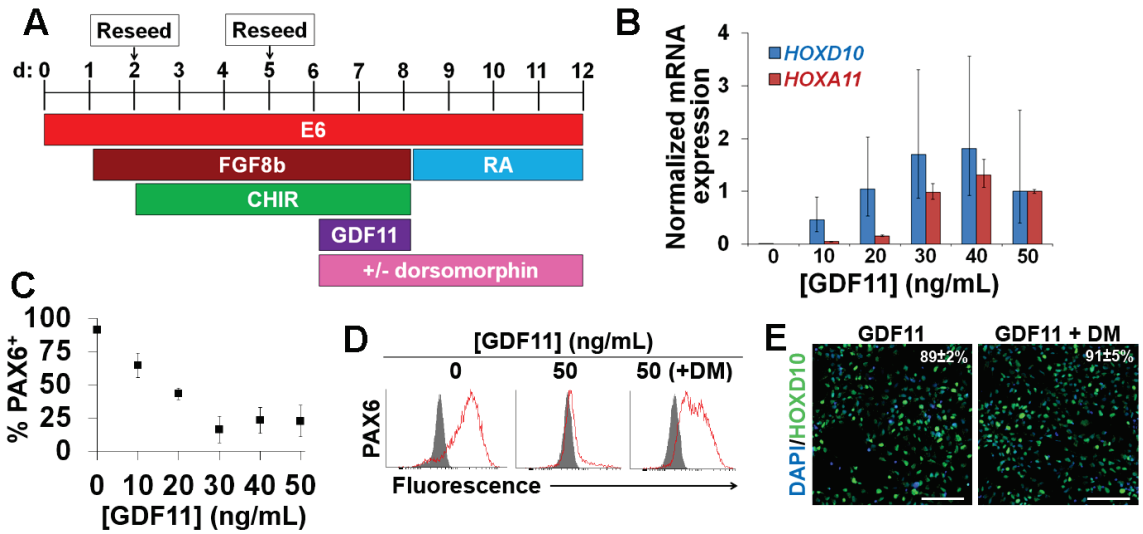


**Figure S3. Dorsomorphin is required during GDF11 treatment to achieve Pax6 expression after RA treatment, related to Figure 3. (A)** Timeline of differentiation. All analyses were conducted at day 12. **(B)** qPCR assessment of lumbosacral gene expression. Data are presented as mean ± S.D. from technical duplicates normalized to the maximum GDF11 dose. **(C)** Expression of PAX6 in response to increased GDF11 concentrations. Data were collected by flow cytometry and presented as mean ± S.D. from biological duplicates. SOX2 was uniformly expressed regardless of GDF11 treatment (data not shown). **(D)** Flow cytometry histograms demonstrating that the addition of dorsomorphin (DM) is sufficient to recover PAX6 expression (83±4% $PAX6^{+}$). Grey histograms, IgG control; Red histograms, PAX6. **(E)** Immunocytochemistry at day 12 indicates dorsomorphin does not affect the acquisition of HOXD10. Percentages are listed as mean ± S.D. calculated from 2 fields per sample (technical replicates, minimum 2000 cells counted). Scale bars, 100 μm.

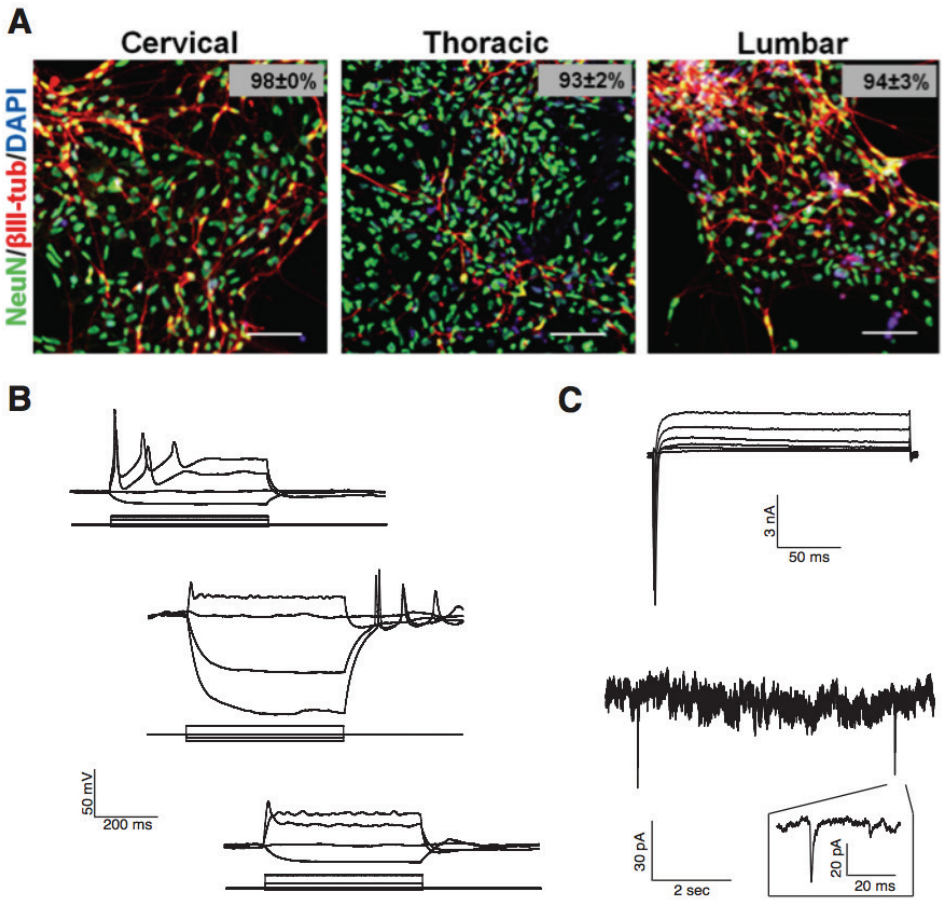


**Figure S4. NeuN quantification and electrophysiology after neuronal maturation, related to Figure 4. (A)** Samples were differentiated according to Figure 4C. Scale bars, 100 μm. Percentages are mean ± S.D. calculated from 2-4 fields per sample (technical replicates, minimum 1000 cells counted). **(B)** Samples were differentiated for >2 months prior to current clamp characterization of membrane properties (see Experimental Procedures for details). Examples of the three classes of action potentials (APs) were observed. Top: Mature APs (observed in 4/18 cells). Middle: Rebound APs triggered at offset of hyperpolarization (observed in 4/18 cells). Bottom: "Abortive" AP indicative of an immature neuron ((Belinsky et al., 2014); observed in 7/18 cells). APs were observed across all conditions (cervical, thoracic, lumbar), with no noticeable difference in basic membrane properties. Resting membrane potentials: -

31±3.9mV. Input resistance: 1±1.6 GΩ. Specific capacitance: 14.38±1.8pF. **(C)** Voltage clamp characterization of ionic and synaptic currents. Examples of whole-cell currents in response to incrementing 500ms voltage steps (top). Spontaneous quantal synaptic currents (bottom) were observed in 6/11 cells tested across all conditions.

**Table S1.** Proteins identified at a 1% FDR and TMT quantitation values. This information is located in the attached spreadsheet.

**Table S2**. Primary antibody list.

| Antigen | Host species | Clone or product # | Dilution | Vendor |
|---|---|---|---|---|
| SOX2 | Mouse | 10H9.1 | 1:1000 (FC)<br>1:500 (ICC) | Millipore |
| Brachyury | Goat | AF2085 | 1:200 (FC)<br>1:500 (ICC) | R&D Systems |
| PAX6 | Mouse | N/A | 1:200 (FC) | DSHB |
| HOXB1 | Sheep | AF6318 | 1:100 (ICC) | R&D Systems |
| HOXB4 | Rat | I12 | 1:50 (ICC) | DSHB |
| PAX6 | Rabbit | PRB-278P | 1:500 (ICC) | Covance |
| N-cadherin | Mouse | 32 | 1:500 (ICC) | BD Biosciences |
| OTX2 | Goat | AF1979 | 1:500 (ICC) | R&D Systems |
| HOXD10 | Goat | N/A | 1:500 (ICC) | R&D Systems |
| βIII-tubulin | Rabbit | PRB-435P | 1:1000 (ICC) | Covance |
| NF-H | Mouse | SMI-32R | 1:1000 (ICC) | Covance |
| Synapsin | Rabbit | AB1543 | 1:250 (ICC) | Millipore |
| NeuN | Mouse | A60 | 1:100 (ICC) | Millipore |
| HB9 | Mouse | 81.5C10 | 1:50 (ICC) | DSHB |
| ISL1 | Mouse | 39.4D5 | 1:100 (ICC) | DSHB |
| ISL1 | Goat | AF1837 | 1:500 (ICC) | R&D Systems |
| FOXP1 | Rabbit | ab16645 | 1:20,000 (ICC) | Abcam |

**Table S3**. Primer sequences used for RT-PCR.

| Gene | Primer sequence |
|---|---|
| *GAPDH* | F: CACCGTCAAGGCTGAGAACG<br>R: GCCCCACTTGATTTTGGAGG |
| *SOX2* | F: TGGACAGTTACGCGCACAT<br>R: CGAGTAGGACATGCTGTAGGT |
| *T* | F: CTTCCCTGAGACCCAGTTCA<br>R: CAGGGTTGGGTACCTGTCAC |
| *OTX2* | F: CCAGACATCTTCATGCGAGAG<br>R: GGCAGGTCTCACTTTGTTTTG |
| *HOXA1* | F: AAATCAGGAAGCAGACCCAC<br>R: GTAGCCGTACTCTCCAACTTTC |
| *HOXB4* | F: TACCCCTGGATGCGCAAAGTTC<br>R: TGGTGTTGGGCAACTTGTGG |
| *HOXC5* | F: ACAGATTTACCCGTGGATGAC<br>R: AGTGAGGTAGCGGTTAAAGTG |
| *HOXC6* | F: GAATGAGGGAAGACGAGAAAGAG<br>R: CATAGGCGGTGGAATTGAGG |
| *HOXC8* | F: TTTATGGGGCTCAGCAAGAGG<br>R: TCCACTTCATCCTTCGGTTCTG |
| *HOXC9* | F: AGCACAAAGAGGAGAAGGC<br>R: CGTCTGGTACTTGGTGTAGG |

**Table S4.** Taqman primers used for qPCR.

| Gene | Life Technologies Assay ID |
|---|---|
| *RPS18* | Hs01375212_g1 |
| *CTNNB1* | Hs00355049_m1 |
| *HOXA1* | Hs00939046_m1 |
| *HOXA2* | Hs00534579_m1 |
| *HOXA3* | Hs00601076_m1 |
| *HOXA4* | Hs01573270_m1 |
| *HOXA5* | Hs00430330_m1 |
| *HOXA6* | Hs00430615_m1 |
| *HOXA7* | Hs00600844_m1 |
| *HOXA9* | Hs00266821_m1 |
| *HOXA10* | Hs00172012_m1 |
| *HOXA11* | Hs00194149_m1 |
| *HOXB1* | Hs00157973_m1 |
| *HOXB2* | Hs00609873_g1 |
| *HOXB4* | Hs00256884_m1 |
| *HOXB5* | Hs00357820_m1 |
| *HOXB6* | Hs00980016_m1 |
| *HOXB7* | Hs00270131_m1 |
| *HOXB8* | Hs00256885_m1 |
| *HOXB9* | Hs00256886_m1 |
| *HOXC4* | Hs00205994_m1 |
| *HOXC5* | Hs00232747_m1 |
| *HOXC6* | Hs00171690_m1 |
| *HOXC8* | Hs00224073_m1 |
| *HOXC9* | Hs00396786_m1 |
| *HOXC10* | Hs00213579_m1 |
| *HOXC11* | Hs00204415_m1 |
| *HOXC12* | Hs00545229_m1 |
| *HOXD1* | Hs00707081_s1 |
| *HOXD3* | Hs00232506_m1 |
| *HOXD4* | Hs00429605_m1 |
| *HOXD8* | Hs00251905_m1 |
| *HOXD9* | Hs00610725_g1 |
| *HOXD10* | Hs00157974_m1 |
| *HOXD11* | Hs00360798_m1 |
| *HOXD12* | Hs00706957_s1 |

**Supplemental Experimental Procedures**

**Mass spectrometry**

Pelleted cells were lysed in 8 M urea, 50 mM Tris (pH 8.0), 50 mM sodium chloride, and protease inhibitor (Roche) by glass bead milling (Retsch) for 40 min (8 cycles of 4 min shaking, 1 min resting). The lysate was centrifuged at 10,000 x g for 5 min to remove cell debris. Protein content was measured using a BCA assay (Thermo Pierce). Disulfide bonds were reduced and alkylated using 5 mM dithiothreitol and 10 mM iodoacetamide. The alkylating reaction was then quenched with 5 mM dithiothreitol. Samples were diluted to 1.5 M urea and digested with trypsin (Promega) overnight at a 1:100 enzyme to protein ratio. Peptides were then desalted using tC18 solid-phase extraction columns (SepPak, Waters) and dried under vacuum.

Peptides were labeled with TMT 10plex isobaric labeling reagents (Thermo Scientific). Briefly, 0.8 mg of reagent was re-suspended in 50 uL acetonitrile and added to 200 µg peptides re-suspended in 100 µL of 200mM TEAB, and shaken for 2 h. To ensure each sample contributed the same amount of protein, aliquots of each sample were mixed at a 1:1:1:1:1:1:1:1:1 ratio (9plex) according to BCA assay results and reporter ions from this mixture were used to inform the subsequent mixture ratio. Labeling reactions were then quenched with hydroxylamine. Samples were mixed according to reporter ion ratios, desalted, and dried under vacuum.

Peptides were re-suspended in reverse phase buffer A (20 mM ammonium formate; pH10). Buffer B contained 20 mM ammonium formate in 80% acetonitrile at pH 10. Separations were performed using a Surveyor liquid chromatography pump (Thermo Scientific) with a Gemini C18 column (250 mm x 4.60 mm; Phenomenex). Peptides were eluted using the following gradient: 0-4 min, 100% buffer A, 4-8 minutes 2-16% buffer B, 8-12 minutes 16-30% buffer B, 12-32 minutes 30%-55% buffer B, all at a flow rate of 0.8 mL $min^{-1}$. Samples were collected from 10 to 40 min. Finally, the column was held at 100% buffer B for 10 min and then

re-equilibrated. Fractions were dried under vacuum and re-suspended in 0.2% formic acid for mass spectrometry analysis.

LC-MS was performed on a Thermo Orbitrap Fusion coupled to a nanoAcquity UPLC (Waters). Mobile phase A comprised water, 0.2% formic acid, and 5% DMSO and mobile phase B comprised acetonitrile, 0.2% formic acid, and 5% DMSO. Peptides were separated on a 75 µm inner diameter fused silica capillary packed with 1.7 um diameter, 130 A pore size Bridged Ethylene Hybrid C18 particles (Waters) heated to 60 °C. Samples were loaded onto the column for 12 min at 0.35 µl/min. Mobile phase B increased to 4% at 0.1 min, 12% at 32 min, 22% at 60 min, and 30% at 70 min. The column was then washed for 5 minutes at 70% B and re-equilibrated for 20 min at 0% B. Eluting peptides were converted to gas phase ions by electrospray ionization.

The mass spectrometer instrument method consisted of isolation at 0.7 Th with the quadrupole, HCD fragmentation with normalized collision energy of 37, and analysis with the orbitrap at 60K resolution at 200 *m/z*. Automatic Gain Control targets were set at $10^5$ with max injection time of 60 ms. Precursors with a charge state of 2-8 could be sampled for MS (Nesvizhskii and Aebersold, 2005). Monoisotopic precursor selection was enabled. Dynamic exclusion was set to 30 s with a 10 ppm tolerance around the precursor.

Raw data were analyzed using Coon OMSSA Proteomic Analysis Software Suite (COMPASS) (Wenger et al., 2011). Briefly, DTA files were generated by extracting peak information from .Raw files. Spectra were searched against Uniprot human reference proteome using Open Mass Spectrometry Search Algorithm. Search parameters include a 75 ppm precursor mass tolerance, 0.03 da product ion tolerance, and up to three missed cleavages. Carbamidomethylation of cysteines and TMT modification of lysines and the N terminus were set as fixed modifications while oxidation of methionines was set as a variable modification. Peptides and proteins were filtered to a 1% FDR. Peptide and protein quantification was performed using TagQuant as described previously. Briefly, extracted reporter ion intensities

were purity corrected and normalized such that the total signal from each channel is equal. A list of all detected proteins is provided in Table S1.

**Flow cytometry**

Flow cytometry was conducted as previously described (Lippmann et al., 2014). Primary antibodies are listed in Table S2. Samples were run on a FACSCalibur (BD Biosciences) and data were analyzed using Cyflogic software. Positive events were quantified by gating above the top 1% of species-matched IgG controls.

**Immunocytochemistry**

Immunocytochemistry was conducted as previously described (Lippmann et al., 2014). Primary antibodies are listed in Table S2. Samples were visualized on a Nikon Ti-E epifluorescence microscope or a Nikon A1R confocal microscope. For $HOXD10^+$ cells in Figure 3D and Figure S3E, positive labeling was quantified relative to DAPI nuclear stain by manual counting using ImageJ software. For $FOXP1^+$ motor neurons in Figure 4B, images were quantified by manually counting the number of $ISL1^+$ or $HB9^+$ cells that co-expressed FOXP1 per field using ImageJ. For HOXB1 and HOXB4 in Figure 3C, positive labeling was quantified relative to DAPI using CellProfiler software (Carpenter et al., 2006). HOXB1 and HOXB4 expression were quantified within $HB9^+$ motor neurons in Figure 4A by manual counting using ImageJ software.

**RT-PCR and qPCR**

Total RNA was extracted from cultured cells using Trizol (Life Technologies) according to the manufacturer's instructions. DNase (Roche) was used to eliminate genomic DNA during the isolation process. After isolation, 1-5 µg of total RNA was immediately subjected to reverse transcription using the Thermoscript RT-PCR kit (Life Technologies) in a 20 µL reaction according to the manufacturer's instructions. Resultant cDNA was diluted and utilized for RT-PCR (conducted as previously described (Lippmann et al., 2014); see Table S3 for primer sequences) or qPCR on a BioRad CFX96 detection unit using Taqman Gene Expression

Master Mix (Life Technologies) and Taqman primers (Life Technologies; see Table S4 for primer list). $\Delta\Delta C_t$ values for each gene were calculated relative to *RPS18* and converted to fold difference assuming 100% primer efficiency.

**Electrophysiology**

Cells were moved to a recording chamber perfused with a bath solution containing 128 mM NaCl, 5 mM KCl, 25 mM HEPES, 30 mM D-glucose, 1 mM $MgCl_2$ and 2 mM $Ca^{2+}$ (pH 7.4, adjusted to 300-310 mOsm with D-glucose). Borosilicate glass pipettes were pulled to a resistance of 4-6 MΩ and filled with an intracellular solution (pH 7.4) containing 130 mM K-gluconate, 10 mM HEPES, 5 mM Na-phosphocreatine, 2 mM Mg-ATP, 1 mM EGTA, and 0.3 mM Na-GTP. All experiments were conducted at room temperature. Whole-cell patch-clamp recordings were made with an Axon MultiClamp 700b amplifier (Molecular Devices). Target cells were identified visually by their neuron-like morphology. Typical seal resistances after achieving the patch were 15MΩ, neurons showing large (+10%) fluctuations in seal quality over the course of an experiment were excluded from the analysis. Measurements of resting membrane potentials (RMPs) were made immediately after achieving whole-cell mode. Liquid junction potentials were not corrected. To measure action potentials, membrane voltage was monitored in response to 500ms current injections, beginning at -100pA, and increasing in 10pA increments to 500pA (or when the membrane response to successive injections began to clearly plateau). Rapidly depolarizing spikes crossing 0mV were considered APs. Cells were held in voltage clamp at -60mV for measurement of spontaneous synaptic activity. To measure whole-cell currents, cells were held at -60mV and current responses were measured following 500ms voltage steps incrementing from -110mV to 110mV in 10mV steps.

**Supplemental References**

Belinsky, G.S., Rich, M.T., Sirois, C.L., Short, S.M., Pedrosa, E., Lachman, H.M., and Antic, S.D. (2014). Patch-Clamp Recordings and Calcium Imaging Followed by Single-Cell PCR Reveal the Developmental Profile of 13 Genes in iPSC-Derived Human Neurons. Stem Cell Res. *12*, 101–118.

Carpenter, A.E., Jones, T.R., Lamprecht, M.R., Clarke, C., Kang, I.H., Friman, O., Guertin, D.A., Chang, J.H., Lindquist, R.A., Moffat, J., et al. (2006). CellProfiler: image analysis software for identifying and quantifying cell phenotypes. Genome Biol. *7*, R100.

Lippmann, E.S., Estevez-Silva, M.C., and Ashton, R.S. (2014). Defined Human Pluripotent Stem Cell Culture Enables Highly Efficient Neuroepithelium Derivation Without Small Molecule Inhibitors. Stem Cells *32*, 1032–1042.

Nesvizhskii, A.I., and Aebersold, R. (2005). Interpretation of Shotgun Proteomic Data The Protein Inference Problem. Mol. Cell. Proteomics *4*, 1419–1440.

Wenger, C.D., Phanstiel, D.H., Lee, M.V., Bailey, D.J., and Coon, J.J. (2011). COMPASS: A suite of pre- and post-search proteomics software tools for OMSSA. PROTEOMICS *11*, 1064–1074.